Sensors & Actuators: B. Chemical 375 (2023) 132883

Contents lists available at ScienceDirect

Sensors and Actuators: B. Chemical

journal homepage: www.elsevier.com/locate/snb

# A novel probe for identifying breast cancer cells based on fluorescence response of the cascade process of biothiol and viscosity

Lihe Zhao [a,c], Hongyu Chu [b], Siqi Zhang [a], Lanlan Xu [a], Bin Yang [a], Pinyi Ma [a,*], Qiong Wu [b,*], Daqian Song [a,*]

[a] College of Chemistry, Jilin Province Research Center for Engineering and Technology of Spectral Analytical Instruments, Jilin University, Qianjin Street 2699, Changchun 130012, China
[b] Nanomedicine Translational Research Center, China-Japan Union Hospital of Jilin University, Sendai Street 126, Changchun 130033, China
[c] Shenzhen Experimental School, Niushan Road 768, Shenzhen 518000, China

ARTICLE INFO

*Keywords:*
Fluorescent probe
Biothiol
Viscosity
Mitochondrial target
Tumor imaging

ABSTRACT

Cancer is life-threatening disease. Surgical removal of tumors is an important procedure in early tumor treatment, and tumor imaging plays an important role in the treatment. Traditional tumor imaging often uses single-factor imaging, in which an enzyme was introduced into cancer cells to turn on the fluorescence of probes. This method, however, has disadvantages such as poor signal and strong interferences. We took advantage of the high GSH content and high viscosity of tumor cells to develop a new type of probe so-called TPQ-G. The developed TPQ-G probe relies on a cascade process. First, TPQ-G reacts with the highly expressed GSH in tumors to generate the fluorescent substance TPQ-OH, which can then be used to sense the high viscosity of the tumors. As a result, the fluorescence intensity was further enhanced, improving the effectiveness of the imaging.

## 1. Introduction

Cancer is a major disease that humans face [1]. With the development of science and technology, researchers have explored a variety of methods to treat cancer, such as surgery, chemotherapy, and radiation therapy [2–4]. Among these methods, surgical treatment is still the method of choice for the treatment of early or relatively early tumors [5–7]. In the process of surgical removal of tumors, surgeons need to distinguish between tumors and normal tissues based on the visual difference between them. The emergence of fluorescent-labeled tumor technology has enabled clinicians to better distinguish diseased tissues from normal tissues [8,9]. However, the existing fluorescent probes have multiple shortcomings such as poor positioning effect and weak luminous intensity, which have limited their application in fluorescent-labeled tumor technology.

In order to better use fluorescence technology to distinguish tumor cells from normal cells, it is crucial to use fluorescent probes that are designed based on the difference between cancer cells and normal cells. Cells are composed of nucleus, cytoplasm, and cell membrane. Animal cytoplasm contains not only mitochondria, Golgi bodies, ribosomes and lysosomes, but also a variety of amino acids, proteins, ATP and other substances that are essential for life [10]. Cells have specific microenvironments such as specific sets of temperature, viscosity, polarity, and pH. Compared with normal cells, cancer cells tend to have lower pH, higher viscosity and biothiol concentration (mainly glutathione (GSH)), as well as higher contents of certain enzymes [11–14]. Thus, it is possible to design fluorescent probes for cancer cell imaging based on these characteristics. However, the design of traditional fluorescent probes is usually based on a single factor. Li and team have developed a new type of polydopamine carbon dots (PDA-CDs), which are surface-modified with EpCAM antibody, for imaging of liver cancer cells [15]. Zhan and colleagues have developed and used a new type of organic small molecule fluorescent probe NBR-AP, of which the fluorescence can be activated by the over-expressed tyrosinase, to image melanoma [16]. Li and coworkers have developed a probe that can simultaneously detect hydrogen peroxide and viscosity; and the two fluorescent signals were used in fluorescence imaging of tumor-bearing mice [17]. However, single-factor-based probes are often easily interfered by interferences, thus are unable to effectively distinguish tumor cells from normal cells in *in vivo* experiments. Some research groups have also developed various new probes that can identify multiple factors for cancer cell imaging; nonetheless [18–21], these factors are often

* Corresponding authors.
*E-mail addresses:* mapinyi@jlu.edu.cn (P. Ma), qiong_wu@jlu.edu.cn (Q. Wu), songdq@jlu.edu.cn (D. Song).

https://doi.org/10.1016/j.snb.2022.132883
Received 6 September 2022; Received in revised form 11 October 2022; Accepted 17 October 2022
Available online 19 October 2022

independent, thus have no superimposing effects on fluorescence imaging [22–28].

In response to this problem, we proposed a new design scheme. The glutathione concentration and viscosity of breast cancer cells are much higher than those of normal breast cells [29–31]. Based on these differences, we designed a probe so-called TPQ-G to distinguish between the two types of cells. This probe was designed based on biothiol (GSH, cysteine (Cys) and homocysteine (Hcy)) and cell viscosity. The probe TPQ-G is a novel organic small molecule probe that can be used to distinguish breast cancer cells from human breast cells by a cascade process (Fig. 1). When the probe is placed in a condition containing a high concentration of biothiol, it interacts with the biothiol and release fluorescent TPQ-OH, which then cause the fluorescence intensity to increase. Additionally, when TPQ-OH is placed in a high-viscosity environment, its fluorescence is further enhanced. Superimposition of the two enhancements, the final fluorescence intensity of the probe can be increased by a hundred folds.

## 2. Experimental section

### 2.1. Synthesis

The synthetic route of TPQ-G is shown in Fig. 2. The substance 1 was synthesized by methods previously published in the literature [32].

#### 2.1.1. Synthesis of TPQ-OH

One hundred and forty milligrams of substance 1 and 100 mg of 8-hydroxyjulolidine-9-carboxaldehyde were dissolved in 20 mL of absolute ethanol. Subsequently, 50 μL of anhydrous piperidine was added and allowed to react at 50 °C for 7 h. The mixture was cooled down to room temperature, and 20 mL of cold water was slowly added to it. The mixture was then extracted with dichloromethane, and the organic layer was dried with anhydrous magnesium sulfate. After that, the solution was filtered, evaporated, and then concentrated. The crude product was purified by column chromatography using a silica gel column ($V_{Dichloromethane}$: $V_{Methanol}$ = 10:1). $^1$H NMR (500 MHz, Methanol-$d_4$) $^1$H NMR (500 MHz, Methanol-$d_4$) δ 8.28 (d, $J$ = 15.4 Hz, 1 H), 7.98 (d, $J$ = 7.9 Hz, 1 H), 7.83 (d, $J$ = 8.4 Hz, 1 H), 7.69 (t, $J$ = 7.7 Hz, 1 H), 7.56 (t, $J$ = 7.7 Hz, 1 H), 7.40 (s, 1 H), 7.30 (d, $J$ = 14.7 Hz, 1 H), 4.07 (s, 3 H), 3.41 (dt, $J$ = 14.9, 5.7 Hz, 4 H), 2.75 (t, $J$ = 6.4 Hz, 2 H), 2.67 (t, 2 H), 1.98 (s, 4 H). $^{13}$C NMR (151 MHz, DMSO-$d_6$) δ 170.10, 156.69, 150.33, 144.93, 142.48, 128.90, 127.39, 126.88, 126.32, 123.89, 116.98, 115.34, 112.11, 106.80, 102.05, 50.42, 49.70, 35.14, 27.22, 21.57, 21.18, 20.56. MS (ESI, $m/z$) Calcd for $[C_{22}H_{23}N_2OS]^+$: 363.1526, found: 363.3413 (Fig. S1, S3 and S5).

#### 2.1.2. Synthesis of TPQ-G

TPQ-OH (20 mg) and 2,4-dinitrobenzenesulfonyl chloride (21 mg) were dissolved in 5 mL of anhydrous dichloromethane (Fig. 2). After 20 μL of triethylamine was added, the mixture was stirred at room temperature for 8 h. After cooling down to room temperature, the mixture was slowly added with 20 mL of cold water. The mixture was extracted with dichloromethane, and the obtained organic layer was dried with anhydrous magnesium sulfate. Subsequently, the solution was filtered, evaporated, and then concentrated. The crude product was purified by column chromatography on a silica gel column ($V_{Dichloromethane}$: $V_{Methanol}$ = 10:1). $^1$H NMR (500 MHz, DMSO-$d_6$) δ 9.16 (d, $J$ = 2.2 Hz, 1 H), 8.63 – 8.53 (m, 1 H), 8.43 – 8.33 (m, 1 H), 8.23 (d, $J$ = 8.0 Hz, 1 H), 8.12 – 8.04 (m, 1 H), 7.89 (s, 1 H), 7.79 (t, $J$ = 7.8 Hz, 1 H), 7.70 (t, $J$ = 7.7 Hz, 1 H), 7.58 – 7.46 (m, 2 H), 4.17 (s, 3 H), 3.41 (dt, $J$ = 18.2, 5.3 Hz, 4 H), 2.80 (t, $J$ = 5.9 Hz, 2 H), 2.61 (t, 2 H), 2.00 – 1.77 (m, 4 H). $^{13}$C NMR (151 MHz, DMSO-$d_6$) δ 170.88, 151.78, 148.89, 148.46, 146.83, 142.40, 141.38, 133.54, 132.50, 129.50, 128.57, 128.09, 127.23, 127.05, 124.31, 122.10, 121.77, 116.43, 114.59, 113.31, 107.24, 50.11, 49.62, 36.01, 27.29, 22.63, 20.70, 20.09. MS (ESI, $m/z$) Calcd for $[C_{28}H_{25}N_4O_7S_2]^+$: 593.1159, found: 593.4390 (Fig. S2, S4 and S6).

### 2.2. General procedure for fluorescence measurements

A certain amount of TPQ-G was dissolved in DMSO to prepare a 1 mM stock solution. The solution was then divided into multiple 1 mL portions. Each portion was placed in a centrifuge tube, which was then stored in a refrigerator at − 40 ℃ until subsequent use. Different amino acids (Cys, Hcy, GSH, Phe, Ser, Tyr, Trp, Lys, Pro, Gly, Arg, Met, Glu, Leu, His, Thr, Val, Asp) and cations ($Na^+$, $Al^{3+}$, $Zn^{2+}$, $Fe^{3+}$, $Fe^{2+}$, $Cu^{2+}$) were dissolved in water to prepare various solutions. After mixing glycerin and water at different proportions to prepare a series of solutions, the viscosity of the system was measured using a viscometer. TPQ-G solution (10 μL) was mixed with a certain amount of PBS buffer (10 mM, pH = 7.4), DMSO and the test substance in a 1-mL centrifuge tube to prepare a solution containing a certain concentration of the test substance ($V_{PBS}$:$V_{DMSO}$ = 99:1, TPQ-G = 10 μM). Then, an ultraviolet-visible spectrometer was employed to measure the absorption spectrum of the sample at a range of 300 – 900 nm; a fluorescence spectrometer was employed to measure the fluorescence spectrum under an excitation wavelength ($\lambda_{ex}$= 560 nm).

## 3. Results and Discussion

### 3.1. Design of TPQ-OH and TPQ-G

We connected the fluorophore TPQ-OH with the recognition group 2,4-dinitrobenesene sulfonyl chloride in order to construct a new probe TPQ-G. During the probe design, we considered that traditional probes mostly use single factors to induce the fluorescence. Additionally, only a

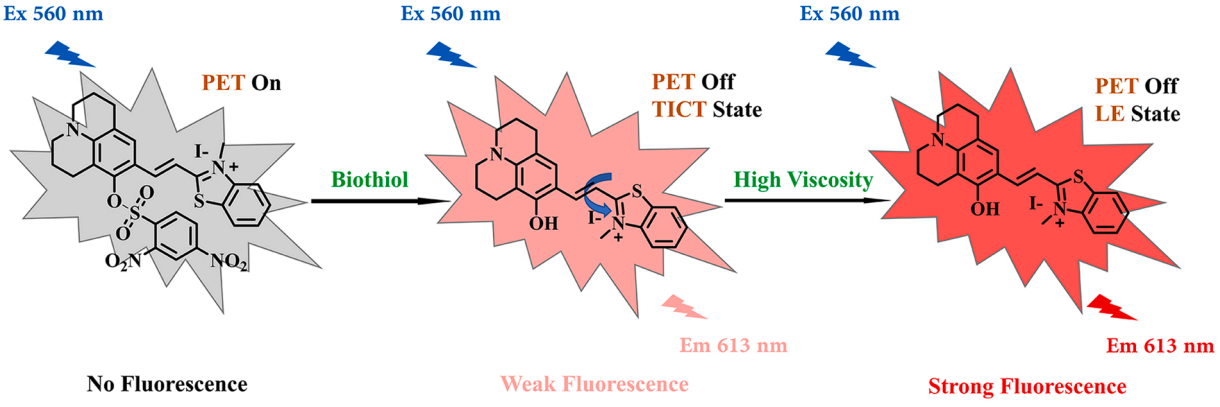


**Fig. 1.** Proposed sensing mechanism of TPQ-G.

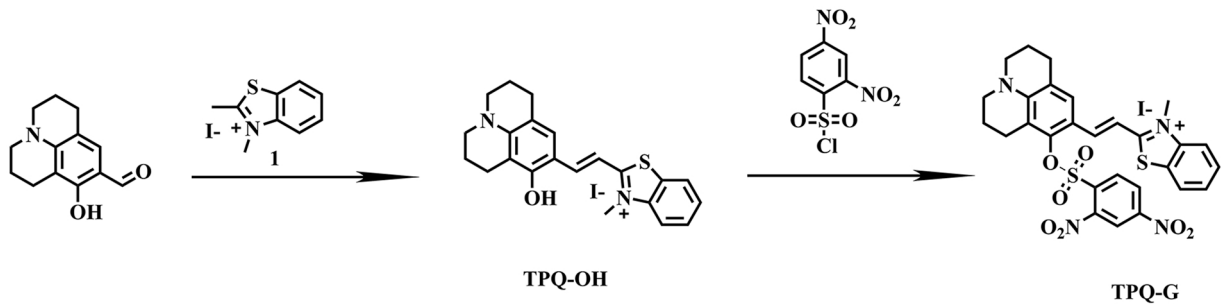


**Fig. 2.** Synthesis of TPQ-G.

few probes can respond to two factors, and these factors often have parallel relationships. In our design, we used two factors in cells: the first factor induced the initial fluorescence signal, and the second factor further enhanced the signal. Cancer cells often have higher GSH concentrations and greater viscosity compared to normal cells. Therefore, we designed a new type of probe TPQ-G that could first respond to cellular GSH to generate TPQ-OH, and when presented in an environment with high viscosity, TPQ-OH had enhanced fluorescence intensity. Based on these two steps, the fluorescence intensity of the second fluorescence enhancement was hundred times higher than initial probe.

### 3.2. Spectral response of TPQ-G in the presence of GSH

First, we measured the changes in the UV-Vis spectra of TPQ-G in the absence and presence of GSH. As shown by the black line in Fig. 3A, the absorption peak of TPQ-G was located at 546 nm. After the addition of GSH, the absorption peak was significantly red-shifted, and the intensity of the absorption peaks at 572 nm was significantly increased. We then explored the fluorescence spectra of TPQ-G before and after the addition of GSH. As shown in Fig. 3B, after TPQ-G was excited by light at a wavelength of 560 nm, the intensity of the emission spectrum was low. After the addition of GSH to TPQ-G, the fluorescence intensity of the solution was significantly enhanced, and the fluorescence emission band at 613 nm became more obvious. Then, we performed a fluorescence titration. The fluorescence spectrum of TPQ-G was recorded after the addition of GSH at concentrations ranging from 0 to 18 μM. The results showed that as the concentration of GSH increased, the intensity of the emission band gradually increased. The fluorescence intensity became stable when the probe reached its upper reaction limit at a GSH concentration of 12 μM. According to Fig. 3C, the probe had a good linear relationship (R = 0.9955) with GSH concentrations of 0–5 μM. The limit of detection (LOD) with respect to GSH of the probe was 0.019 μM (S/N = 3) which is lower than that obtained for other fluorescent probes (Table S1).

We further explored the change of fluorescence with viscosity of the probe in the presence of GSH. As predicted, the fluorescence was further enhanced as the viscosity increased. First, the UV-Vis spectra of TPQ-G in GSH were measured in an environment with high and low viscosity.

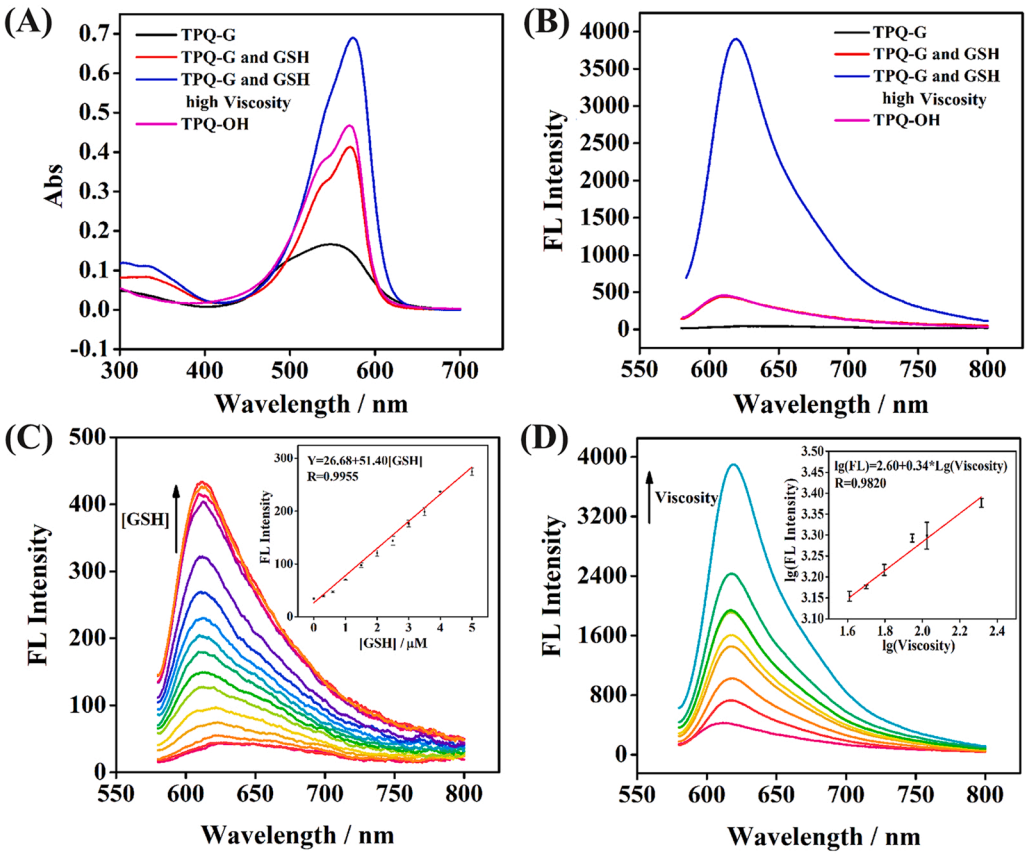


**Fig. 3.** Absorption (A) and fluorescence ($\lambda_{ex}$ = 560 nm) (B) response of TPQ-G, TPQ-G in the presence of GSH, TPQ-G in the presence of GSH in high-viscosity environment, and TPQ-OH. (C) Fluorescence response of TPQ-G in the presence of GSH at various concentrations in PBS/DMSO solution (99:1, v/v, 10 mM PBS, pH 7.4; $\lambda_{ex}$ = 560 nm, $\lambda_{em}$ = 613 nm). (D) Fluorescence response of TPQ-G in the presence of GSH in an environment with different viscosities ($\lambda_{ex}$ = 560 nm, $\lambda_{em}$ = 613 nm).

As shown in Fig. 3A, at low viscosity, the probe exhibited an absorption peak at 572 nm, whereas at high viscosity, the absorption peak was red-shifted to 576 nm. We then studied the emission spectrum of TPQ-G in the presence of GSH. The test temperature was controlled at 37 °C, and the probe concentration was 10 μM. As shown in Fig. 3B, at low viscosity, the fluorescence intensity was low, but when the viscosity was increased, the fluorescence intensity increased significantly. The fluorescence intensity of TPQ-G in the presence of GSH had a linear relationship with viscosity from 1.36 to 62.59 cp. The relationship could be described by Förster–Hoffmann equation:

$$\lg(I) = C + x\lg\eta$$

where $I$ is the emission fluorescence intensity, $C$ is a constant, $x$ is the dye-dependent constant and $\eta$ is the solvent viscosity. In our work, the relationship between viscosity and fluorescence intensity could be described as $\lg(I_{619}) = 2.47 + 0.42\lg(\eta)$ (R = 0.9879) (Fig. 3D). This equation provides the basis that our probe has multiple functions.

### 3.3. Applicability and specificity of TPQ-G to biothiol

To ensure that the probe can be applied to wider research fields, we further explored its performance. First, with the same solvent, the reaction time was optimized. TPQ-G fluorescence is collected every minute after GSH was added. As can be seen in Fig. S7, after 13 min, the fluorescence was stabilized, indicating that the reaction has reached the equilibrium. Therefore, in our subsequent experiments, the incubation time was set at 15 min to ensure that the reaction was complete. The stability of fluorescence of the probe is very important during the detection of GSH and imaging of cells. As shown in Fig. S7, over a period of 0.5 h, significant changes of fluorescence intensity were not observed neither in TPQ-G nor TPQ-OH. This suggests that the probe has excellent stability.

Next, the performance of the probe at different pH values was explored. Fig. S8 shows the fluorescence intensity of the probe in the presence of GSH measured at increasing pH (from pH = 2.3–11.5). The data showed that upon the changes of pH, the intensity of the fluorescence emission peak at 613 nm became fluctuated. However, when the probe was in an environment with pH values of 2.3–7.4, the intensity of the fluorescence band at 613 nm gradually increased; however, when the pH was further increased, the fluorescence intensity began to gradually decrease. This shows that pH = 7.4 is a suitable pH for the probe.

At the above pH and reaction time, we explored the specificity of the probe. As shown in Fig. S9, 18 different amino acids (each at 10 μM) commonly found in blood, 6 different cations (each at 10 μM), 3 different sulfides (each at 10 μM), and 4 different reactive oxygen species (each at 5 μM) were added to TPQ-G (10 μM). Only the addition of biothiol (GSH, Cys and Hcy) to TPQ-G caused a significant increase in the fluorescence intensity. This indicates that the probe has high specificity to biothiol.

### 3.4. Theoretical calculations and reaction mechanism

First, we studied the product of a reaction between TPQ-OH and GSH. The mass spectrum of the reaction between TPQ-G and GSH displayed in Fig. S10 showed a peak at a mass-to-charge ratio of 363.3369. This peak corresponded to the mass-to-charge ratio of TPQ-OH. In HPLC analysis of TPQ-G reacted with GSH (Fig. S11), TPQ-G exhibited a peak at 3.97 min and TPQ-OH at 4.74 min. In the presence of a certain concentration of GSH, TPQ-G exhibited peaks both at 4.01 min and 4.71 min, which was approximate with the retention time of TPQ-G and TPQ-OH. It is a proof that TPQ-OH was indeed produced as a result of the reaction of TPQ-G and GSH.

To better describe the change of spectra before and after the addition of GSH, we further carried out theoretical calculations. The frontier molecular orbitals and the energy level transitions of TPQ-G are shown in Fig. 4 A. As illustrated, the first singlet transition of TPQ-G was dominated by the HOMO→LUMO+ 1 transition. This transition then caused the quenching of TPQ-G fluorescence due to the transfer of an electron from an excited donor to an electronic unit of the LUMO caused by a process called 'donor-excited photoinduced electron transfer' (D-PET). After the 2,4-dinitrobenesene sulfonyl group was removed, the D-PET process was diminished, and the fluorescence was then recovered.

To further shed light on the observed relationship between fluorescence enhancement and viscosity and to provide a reasonable explanation to the relationship, molecular rotation simulation was performed (Fig. 4B). At the ground state ($S_0$), the structure of TPQ-OH was nearly planar. The HOMO and LUMO were located in the entire molecule and had local excitation (LE) properties. For the S1 state, the fluorophore underwent a transition from the initial LE state to the TICT state. For the TPQ-OH in its 90° (or −90°)-twisted excited state, the HOMO was located on the julolidine group, while the LUMO was located in the benzothiazole group, causing the apparent charge separation. Consequently, the TICT states of the rotors could inhibit the fluorescence emission of TPQ-OH. To explain whether the TICT process of TPQ-OH is spontaneous, the changes in the potential energy of the $S_0$ and $S_1$ states of TPQ-OH as a function of the dihedral angle θ were calculated. As shown in Fig. 4B, the occurrence of TICT states was spontaneous. This result suggests that the enhancement of fluorescence intensities of TPQ-OH in high viscosity medium is caused by the TICT process, which can inhibit the rotation of the molecule.

### 3.5. Cytotoxicity and fluorescence imaging of cells

To show that the probe TPQ-G can be used *in vivo*, we studied its cytotoxicity using the CCK8 assay (Fig. S12). The viability of MCF-10A cells cultured separately with 10 μM TPQ-G at 37 ℃ for 24 h was about 80%. This indicates TPQ-G has low cytotoxicity.

### 3.6. Imaging of endogenous GSH in normal cells and cancer cells

First, we stained MDA-MB-231 cells (breast cancer cells) with TPQ-G, and then observed the cells under a confocal microscope. The cells produced strong red light under light at the defined excitation wavelength (Fig. 5 A). Then, for another group of MDA-MB-231 cells, we first used NEM to shield the original biothiol in the cells and then stained the cells with TPQ-G. The observation showed that the cells did not exhibit obvious fluorescence. In the third set of experiment, we used NEM to shield the original biothiol in the cells, cultured the cells in GSH-containing PBS, and then stained the cells with TPQ-G. We observed that the cells exhibited obvious red fluorescence. Subsequently, we employed the same procedure to stain MCF-10A cells (normal breast cells) and obtained a similar outcome. However, as shown in Fig. 5B, we found that for endogenous GSH, the fluorescence intensity of stained cancer cells was much higher than that of normal cells. For the same concentration of exogenous GSH, the fluorescence intensity of TPQ-G stained cancer cells and normal cells was basically the same. Based on these results, it is clear that the difference between GSH content in cancer cells and that in normal cells leads to the obvious difference between the fluorescence intensity of the two types of cells.

To study whether the viscosity of cells has an effect on the fluorescence enhancement of stained cells, we carried out a follow-up verification experiment. We hypothesize that the probe TPQ-G should generate TPQ-OH after interacting with GSH, and the fluorescence intensity of TPQ-OH should increase as the viscosity increases. As shown in Fig. 5 C, we used nystatin to induce apoptosis of MCF-10A cells, and at the same time, we stained the cells with TPQ-OH. During cell apoptosis, the viscosity of the cells gradually increased, and at the same time, we observed that the fluorescence intensity significantly increased (Fig. 5D).

It is known that the viscosity of cancer cells is higher than that of

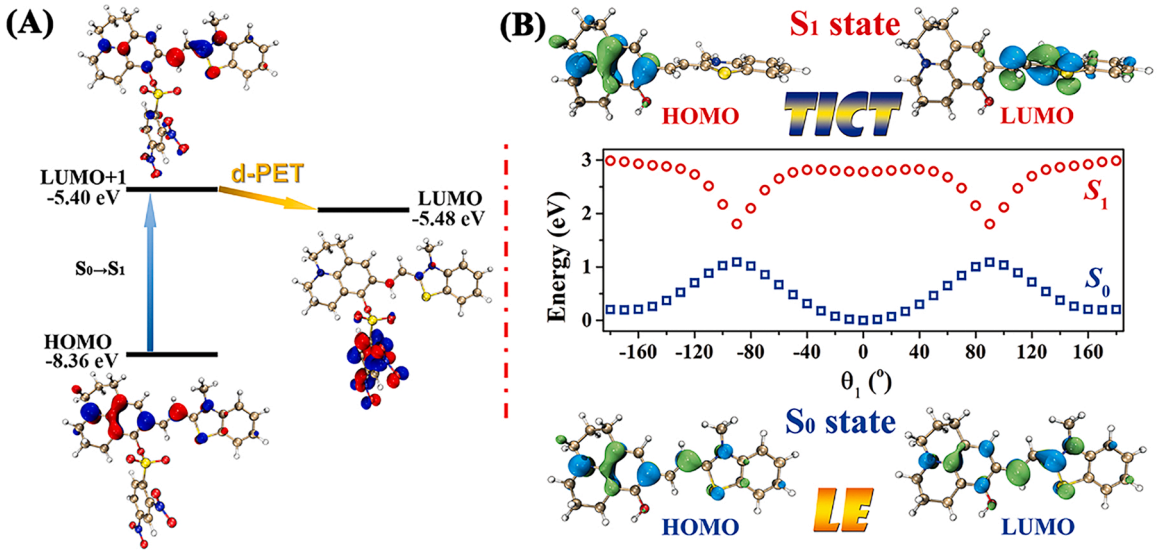


**Fig. 4.** (A) Theoretical models illustrating the HOMO, LUMO and LUMO+ 1 energy level, and relevant frontier molecular orbitals of TPQ-G at the TDDFT levels. (B) The TDDFT calculations of the LE→TICT photoreaction represented by a plot of S0 and S1 energy versus rotation angle as the formation of LE/TICT excited states progressed.

normal cells. This indicates that the increase of fluorescence intensity of cancer cells after being stained with the probe TPQ-G is due to the relatively high viscosity of the cancer cells, causing the probe to undergo a cascade process after reacting with GSH during the first step. As a result, we could observe that the fluorescence intensity was further enhanced.

### 3.7. Colocalization of the probe

To better understand the behavior of the probe in cells, we explored the localization of the probe in cells. As shown in Fig. 5E, we first stained MDA-MB-231 cells with MitoTraker Green (mitochondrial green fluorescent probe); and after washing with PBS, the cells were stained with TPQ-G. The green and red fluorescence of cells had a high overlap ratio (Pearson's R value = 0.95). We also stained MDA-MB-231 cells with LysoTraker Green (lysosomal green fluorescent probe), washed with PBS, and then stained with TPQ-G. The overlap ratio of the green and red fluorescence of cells was low (Pearson's R value = 0.79). Finally, we stained MDA-MB-231 cells with Hochest (blue fluorescent probe of nucleus), washed with PBS, and then stained with TPQ-G. The results showed that there was no overlap between the blue and red fluorescence of cells (Pearson's R value = 0). The above observations suggest that TPQ-G is localized around the mitochondria of cells.

### 3.8. Ability of TPQ-G to distinguish between MDA-MB-231 and MCF-10A cells

We attempted to distinguish between MCF-10A (normal cells) and MDA-MB-231 (cancer cells) cells in a mixed culture using TPQ-G. As shown in Fig. 5 F, MCF-10A and MDA-MB-231 were first mixed and cultured in a cell culture dish. After washing with PBS, the first group of cells was stained with TPQ-G (10 μM), while the second group was stained with TPQ-OH (10 μM). After 15 min, the dye was removed and an appropriate amount of PBS was added. The observation of the TPQ-G-stained cells under a confocal microscope showed that about half of cells were stained with TPQ-G, whereas the other half was unstained. For the TPQ-OH-stained group, most cells in this group were stained. We speculated that for cells in the TPQ-G group, the stained cells (those that generated fluorescence signal) were MDA-MB-231 cells, whereas the unstained cells (those that did not generate fluorescence) were MCF-10A cells.

To further verify our conjecture, we employed the same imaging procedure to image mouse breast cancer 4T1-Luc cells (Fig. 5 G). The 4T1-Luc cells can generate green fluorescence, and we could use such properties to easily distinguish these cells from normal cells. First, 4T1-Luc cells and MCF-10A cells were co-cultured to prepare cells in the experimental group and the control group. The cells in both groups were then stained with TPQ-G (10 μM) or TPQ-OH (10 μM) using the same method. For cells in the experimental group stained with TPQ-G, we observed the overlap between the red and green fluorescence of the cells; however, the cells in the upper left corner did not exhibit green fluorescence nor red fluorescence. This shows that the probe TPQ-G only stains cancer cells, not normal cells. In the control group, all the cells did not exhibit green fluorescence, but exhibited red fluorescence. These results indicate that TPQ-OH, which does not contain a recognition group, is unable to distinguish between normal cells and cancer cells. On the other hand, TPQ-G, which contains the recognition group and relies on the difference between the GSH concentration and viscosity in cancer cells and normal cells, could distinguish between cancer cells and normal cells by generating strong red fluorescence.

### 3.9. Application of TPQ-G in in vivo tumor imaging

We finally applied the probe in *in vivo* tumor imaging. 4T1-Luc cells were implanted *in situ* in mice. After 7 days, the tumors of mice grew to the size of 150 $mm^3$. We then injected TPQ-G (100 μM in 50 μL of saline) using a syringe into the skin near the tumor site of a mouse. As a control group, we also injected the same dose of TPQ-G to the upper left side of the tumor site. We then observed the mice using Davinch *In vivo* HR imaging system (Davinch K, Korea). As shown in Fig. 5H, after the probe solution was injected, the tumor site exhibited stronger fluorescence compared with that of the non-tumor site. This shows that the probe has good tumor imaging performance. We dissected a tumor-bearing mouse and collected the heart, liver, spleen, kidney and tumor. The organs were then stained with the probe before being subjected to fluorescence imaging. As shown in Fig. 5I, among various organs and tumors, tumors were clearly stained and had the strongest fluorescence. This further proves that the probe has a strong ability to recognize tumors.

## 4. Conclusion

In summary, we designed a new probe TPQ-G for tumor imaging. The

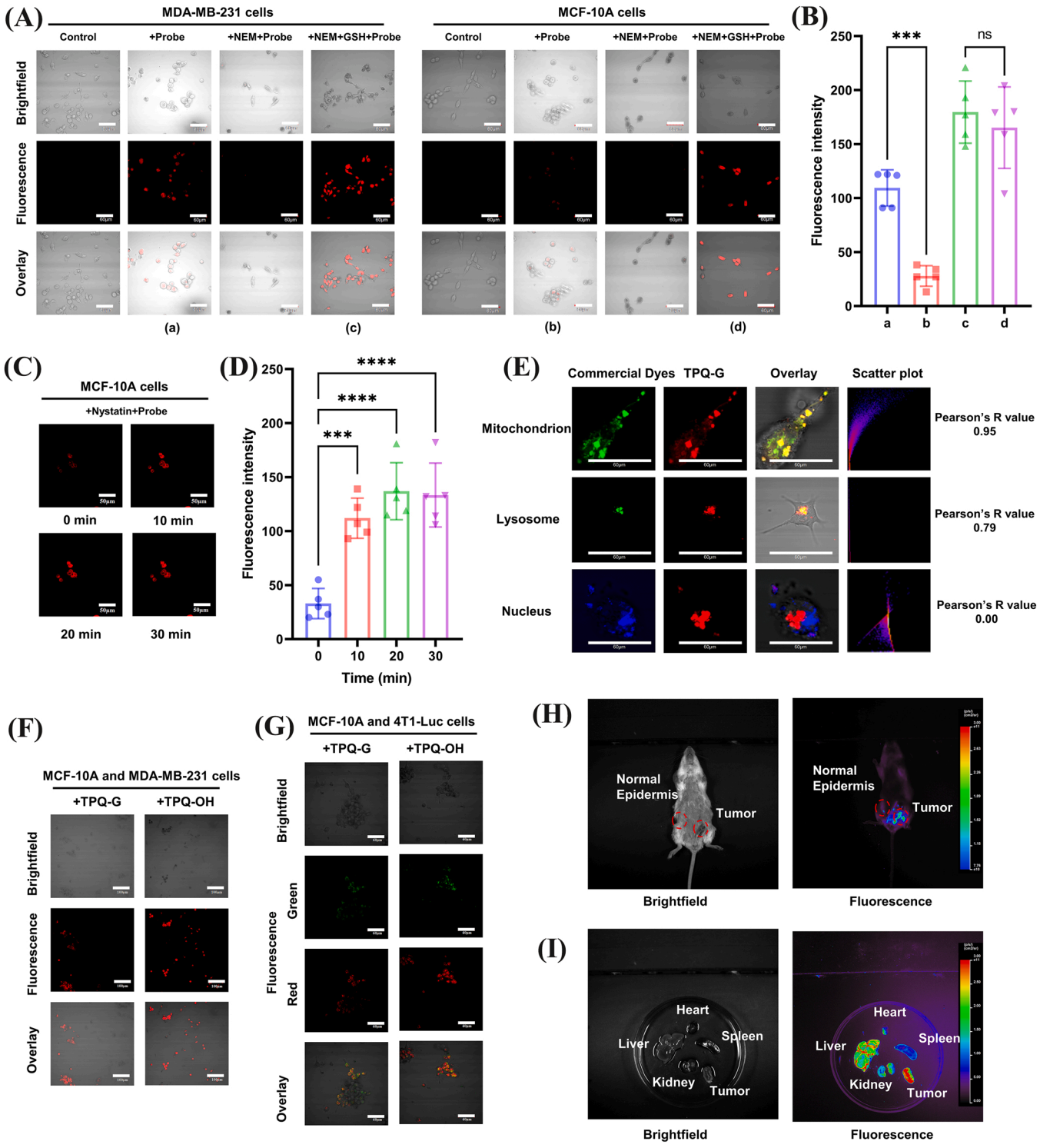


**Fig. 5.** (A) Fluorescence images of MDA-MB-231 cells and MCF-10A cells. Left to right: control; cells treated with TPQ-G (10 μM); cells treated with NEM (1 mM), followed by TPQ-G (10 μM); and cells treated with NEM (1 mM), followed by GSH (10 mM) and TPQ-G (10 μM). Top to bottom: brigbtfield, fluorescence, and overlay. (B) Fluorescence intensity of different treatments in (A). (C) Fluorescence images of MCF-10A treated with nystatin (20 nM), followed by TPQ-G (10 μM) at different times. (D) Fluorescence intensity of different treatments in (C). (E) Colocalization of MitoTracker Green, Lysotraker Green, and Hoechst and TPQ-G in MDA-MB-231 cells. Cells were stained with a commercial day for 15 min, followed by TPQ-G for 10 min (F) Fluorescence images of MCF-10A and MDA-MB-231 cells mixed culture after adding TPQ-G or TPQ-OH. (G) Fluorescence images of MCF-10A and 4T1-Luc cells mixed culture after adding TPQ-G or TPQ-OH. (H) *In vivo* imaging of tumor-bearing mice by probe TPQ-G. (I) Images of organs of mice visualized by probe TPQ-G. Scale bar: 60 μm. (ns = no significant, ***P < 0.001, ****P < 0.0001, data analyses were performed with an independent samples test with equal variances, means ± SD, n = 5).

developed probe had higher water solubility, larger Stokes shifts, higher stability, and higher biocompatibility compared with traditional probes. Our probe could effectively detect GSH and changes in viscosity, and had good linearity in both types of detection. We successfully applied the probe to quantitatively detect both GSH and viscosity. The TPQ-G probe was also satisfactorily used in imaging of cancer cells; its response signal was enhanced as a result of the cascade reaction process. Finally, TPQ-G was used in *in vivo* tumer imaging with satisfactory results. This design method presented in this work may provide a new idea for the design of other probes.

## CRediT authorship contribution statement

**Lihe Zhao**: Conceptualization, Investigation, Data curation, Validation, Writing – original draft preparation. **Hongyu Chu**: Data curation, Investigation. **Siqi Zhang**: Data curation, Investigation. **Lanlan Xu**: Formal analysis and software. **Bin Yang**: Data curation, Investigation. **Pinyi Ma**: Conceptualization, Project administration, Funding acquisition, Data curation, Writing – review & editing and software. **Qiong Wu**: Investigation, Resources, Writing – review & editing, Software. **Daqian Song**: Project administration, Funding acquisition, Resources, Supervision, Analyzed the data and participated in the discussion.

## Declaration of Competing Interest

The authors declare that they have no known competing financial interests or personal relationships that could have appeared to influence the work reported in this paper.

## Data Availability

Data will be made available on request.

## Acknowledgments

This work was supported by the National Natural Science Foundation of China (22004046 and 22074052), the Norman Bethune Program of Jilin University (2022B21), the Natural Science Foundation of Jilin Province (YDZJ202101ZYTS024).

## Appendix A. Supporting information

Supplementary data associated with this article can be found in the online version at doi:10.1016/j.snb.2022.132883.

## References

[1] S. Nik-Zainal, P. Van Loo, D.C. Wedge, L.B. Alexandrov, C.D. Greenman, K.W. Lau, et al., The life history of 21 breast cancers, Cell 149 (2012) 994–1007.
[2] A. Babar, Z. Al-Hilli, F. Covut, P. Chadalavada, D. Attia, T.R. Behera, et al., Retrospective study of clinical outcomes in patients with Stage IV HER2+breast cancer undergoing primary breast surgery, Breast J. 27 (2021) 618–620.
[3] J.R. Moremen, E.N. Skopelja, D.P. Ceppa, The role of induction therapy, J. Thorac. Dis. 6 (2014) S309–S313.
[4] W. Haque, E.B. Butler, B.S. Teh, Stereotactic body radiation therapy for prostate cancer-a review, Chin. Clin. Oncol. 6 (2017) S10.
[5] M. Mueller, Surgery of early-stage NSCLC, J. Thorac. Oncol. 12 (2017) S40–S42.
[6] P. Rema, I. Ahmed, Conservative surgery for early cervical cancer, Indian J. Surg. Oncol. 7 (2016) 336–340.
[7] R. Terra, B. Bibas, R. Haddad, J.R. De-Campos, P.H. Nabuco-De-Araujo, C.E. Lima, et al., Robotic-assisted thoracic surgery for early-stage non-small-cell lung cancer: initial experience in Brazil, J. Thorac. Oncol. 13 (2018) S1018–S1019.
[8] J.C. DeLong, R.M. Hoffman, M. Bouvet, Current status and future perspectives of fluorescence-guided surgery for cancer, Expert Rev. Anticancer Ther. 16 (2016) 71–81.
[9] M.S. Demarchi, B. Seeliger, J.C. Lifante, P.F. Alesina, F. Triponez, Fluorescence image-guided surgery for thyroid cancer: utility for preventing hypoparathyroidism, Cancers 13 (2021) 3792.
[10] T.S. Leeson, Electron microscopy of the cell: cell structure and function, Can. Med. Assoc. J. 93 (1965) 921–932.
[11] L.E. Shimolina, A.A. Gulin, M. Paez-Perez, I. Lopez-Duarte, I.N. Druzhkova, M. M. Lukina, et al., Mapping cisplatin-induced viscosity alterations in cancer cells using molecular rotor and fluorescence lifetime imaging microscopy, J. Biomed. Opt. 25 (2020), 126004.
[12] N. Gupta, S.I. Reja, V. Bhalla, M. Gupta, G. Kaur, M. Kumar, A bodipy based fluorescent probe for evaluating and identifying cancer, normal and apoptotic C6 cells on the basis of changes in intracellular viscosity, J. Mater. Chem. B 4 (2016) 1968–1977.
[13] M.G. Ren, Q.Y. Xu, S.J. Wang, L. Liu, F.G. Kong, A biotin-guided fluorescent probe for dual-mode imaging of viscosity in cancerous cells and tumor tissues, Chem. Commun. 56 (2020) 13351–13354.
[14] R.R. Perry, J.A. Mazetta, M. Levin, S.C. Barranco, Glutathione levels and variability in breast tumors and normal tissue, Cancer 72 (1993) 783–787.
[15] Z. Li, J. Ni, L. Liu, L. Gu, Z. Wu, T. Li, et al., Imaging-guided chemo-photothermal polydopamine carbon dots for EpCAM-targeted delivery toward liver tumor, ACS Appl. Mater. Interfaces 13 (2021) 29340–29348.
[16] C. Zhan, J. Cheng, B. Li, S. Huang, F. Zeng, S. Wu, A. Fluorescent, Probe for early detection of melanoma and its metastasis by specifically imaging tyrosinase activity in a mouse model, Anal. Chem. 90 (2018) 8807–8815.
[17] S. Li, P. Wang, W. Feng, Y. Xiang, K. Dou, Z. Liu, Simultaneous imaging of mitochondrial viscosity and hydrogen peroxide in Alzheimer's disease by a single near-infrared fluorescent probe with a large Stokes shift, Chem. Commun. 56 (2020) 1050–1053.
[18] X. Wei, Y. Zhu, X. Yu, L. Cai, N. Ruan, L. Wu, et al., An endoplasmic reticulum targeting green fluorescent protein chromophore-based probe for the detection of viscosity, Chem. Commun. 58 (2022) 10727–10730.
[19] C. Wang, Y. Wang, G. Wang, S. Chen, C. Huang, Two-isophorone fluorophore-based design of a ratiometric fluorescent probe and its application in the sensing of biothiols, J. Mater. Chem. B 7 (2019) 5633–5639.
[20] X. Li, R. Zhao, Y. Wang, C. Huang, A new GFP fluorophore-based probe for lysosome labelling and tracing lysosomal viscosity in live cells, J. Mater. Chem. B 6 (2018) 6592–6598.
[21] L. Cai, H. Li, X. Yu, L. Wu, X. Wei, T.D. James, et al., Green fluorescent protein GFP-chromophore-based probe for the detection of mitochondrial viscosity in living cells, ACS Appl. Bio Mater. 4 (2021) 2128–2134.
[22] F. Meng, J. Niu, H. Zhang, R. Yang, Q. Lu, G. Niu, et al., A pH-sensitive spirocyclization strategy for constructing a single fluorescent probe simultaneous two-color visualizing of lipid droplets and lysosomes and monitoring of lipophagy, Anal. Chem. 93 (2021) 11729–11735.
[23] Z.P. She, W.X. Wang, W.L. Jiang, Z.Q. Wang, G.J. Mao, J. Fei, et al., Accurate fluorescence diagnosis of cancer based on sequential detection of hydrogen sulfide and pH, Anal. Chem. 93 (2021) 11826–11835.
[24] R. Li, H. Kassaye, Y. Pan, Y. Shen, W. Li, Y. Cheng, et al., A visible and near-infrared dual-fluorescent probe for discrimination between Cys/Hcy and GSH and its application in bioimaging, Biomater. Sci. 8 (2020) 5994–6003.
[25] F.P. Qi, Y. Zhang, B.H. Wang, W.Q. Chen, L. Yang, Z.G. Yang, et al., A fluorescent probe for the dicriminatory detecion of Cys/Hcy, GSH and H2S in living cells and zebrafish, Sens. Actuators B-Chem. 296 (2019), 126533.
[26] Y.Z. Deng, G.Q. Feng, Visualization of ONOO- and viscosity in drug-induced hepatotoxicity with different fluorescence signals by a sensitive fluorescent probe, Anal. Chem. 92 (2020) 14667–14675.
[27] Q.H. Hu, C.M. Yu, X.T. Xia, F. Zeng, S.Z. Wu, A fluorescent probe for simultaneous discrimination of GSH and Cys/Hcy in human serum samples via distinctly-separated emissions with independent excitations, Biosens. Bioelectron. 81 (2016) 341–348.
[28] L. Jia, L.Y. Niu, Q.Z. Yang, Fluorescent probe for simultaneous discrimination of GSH, Cys, and SO2 derivatives, Anal. Chem. 92 (2020) 10800–10806.
[29] C.R. Yang, Y.C. Ou, J.H. Kuo, Y.L. Kao, C.L. Chen, S.Y. Yean, et al., Intracellular glutathione content of urothelial cancer in correlation to chemotherapy response, Cancer Lett. 119 (1997) 157–162.
[30] T. Miran, A.T.J. Vogg, N. Drude, F.M. Mottaghy, A. Morgenroth, Modulation of glutathione promotes apoptosis in triple-negative breast cancer cells, FASEB J. 32 (2018) 2803–2813.
[31] L.E. Shimolina, M.A. Izquierdo, I. Lopez-Duarte, J.A. Bull, M.V. Shirmanova, L. G. Klapshina, et al., Imaging tumor microscopic viscosity in vivo using molecular rotors, Sci. Rep. 7 (2017) 41097.
[32] L. Biesen, N. Nirmalananthan-Budau, K. Hoffmann, U. Resch-Genger, T.J.J. Muller, Solid-state emissive aroyl-S,N-ketene acetals with tunable aggregation-induced emission characteristics, Angew. Chem. Int. Ed. Engl. 59 (2020) 10037–10041.

**Lihe Zhao** is currently a PhD student in College of Chemistry, Jilin University. His interest is spectral analysis.

**Hongyu Chu** is currently a master student in Department of Gastrointestinal and Colorectal Surgery, China-Japan Union Hospital of Jilin University. His interest is biosensor.

**Siqi Zhan** is currently a PhD student in College of Chemistry, Jilin University. Her interest is spectral analysis.

**Lanlan Xu** is currently a PhD student in College of Chemistry, Jilin University. Her interest is spectral analysis.

**Bin Yang** is currently a PhD student in College of Chemistry, Jilin University. His interest is spectral analysis.

**Pinyi Ma** gained his doctor's degree from College of Chemistry, Jilin University in 2017 and he is an associate professor in that school. His research area is spectral analysis.

**Qiong Wu** gained her doctor's degree from College of Chemistry, Jilin University in 2018 and she is an associate professor in China-Japan Union Hospital of Jilin University. Her research area is spectral analysis and biosensor.

**Daqian Song** gained his doctor's degree from College of Chemistry, Jilin University in 2003 and he is a professor in that school. His research areas are spectral and chromatography analysis.